



**HAL**  
open science

# Photoelectric Feedback Mechanism for Acceleration of Runaway Electrons in Gas Discharges at High Overvoltages

Victor P Pasko, Sebastien Celestin, Anne Bourdon

► **To cite this version:**

Victor P Pasko, Sebastien Celestin, Anne Bourdon. Photoelectric Feedback Mechanism for Acceleration of Runaway Electrons in Gas Discharges at High Overvoltages. *Physical Review Letters*, 2024, 133 (23), pp.235301. 10.1103/physrevlett.133.235301 . hal-04825895

**HAL Id: hal-04825895**

**<https://hal.science/hal-04825895v1>**

Submitted on 27 Dec 2024

**HAL** is a multi-disciplinary open access archive for the deposit and dissemination of scientific research documents, whether they are published or not. The documents may come from teaching and research institutions in France or abroad, or from public or private research centers.

L'archive ouverte pluridisciplinaire **HAL**, est destinée au dépôt et à la diffusion de documents scientifiques de niveau recherche, publiés ou non, émanant des établissements d'enseignement et de recherche français ou étrangers, des laboratoires publics ou privés.

Public Domain

# Photoelectric Feedback Mechanism for Acceleration of Runaway Electrons in Gas Discharges at High Overvoltages

Victor P. Pasko,<sup>1,\*</sup> Sebastien Celestin,<sup>2</sup> and Anne Bourdon<sup>3</sup>

<sup>1</sup>*School of Electrical Engineering and Computer Science,  
Penn State University, University Park, Pennsylvania, U.S.A.*

<sup>2</sup>*Laboratory of Physics and Chemistry of the Environment and Space (LPC2E),  
OSUC, University of Orleans, CNRS, Orleans, France*

<sup>3</sup>*Laboratory of Plasma Physics (LPP), CNRS, Sorbonne Université,  
École Polytechnique, Institut Polytechnique de Paris, Palaiseau, France*

(Dated: December 20, 2024)

Energy conservation dictates that an electron with elementary charge  $e$  traversing a vacuum gap formed by electrodes maintained at potential difference  $U$  volts acquires maximum energy of  $eU$ . In many experiments electrons with energies as high as  $3eU$  have been observed. The experimental discovery of this effect was made over 50 years ago and is still a subject of significant controversy in applications related to X-ray generation from high voltage discharges. Here we explain these observations by a sequential increase of energy of runaway electrons released from the cathode due to the photoelectric absorption of bremsstrahlung radiation generated by the previous cycle of runaway electrons bombarding the anode.

Since 1960s many research groups have documented bursts of X-rays from spark discharges in high voltage laboratory experiments [1–9]. The nonequilibrium plasma formed in high voltage pulsed discharges is of interest in various technological applications, including pollution control, pumping of laser media and plasma-assisted combustion [10]. The exact mechanisms of production of high energy runaway electrons responsible for X-ray emissions from these discharges and their energy spectral properties are not understood. This problematics is also relevant to present medical imaging applications of X-rays, production of which is based on vacuum acceleration of electrons produced by thermionic emission [11–13]. The recent work [14] provided quantitative evidence that the X-ray production in laboratory discharges may involve generation of runaway electrons from the cathode material due to the photoelectric absorption of bremsstrahlung radiation generated by runaway electrons bombarding the anode. In this letter we report quantitative results based on detailed Monte Carlo simulations of electron and photon transport indicating that in the gap with applied potential difference  $U$  this feedback process generates a group of high energy runaway electrons with energies significantly exceeding  $eU$  (by a factor of 3 and in good agreement with original work [15] where this effect was discovered). The energy feedback process discussed in this letter corresponds to acceleration of relatively small fraction of electrons to very high energies. This process is different from self-sustaining feedback conditions realized when avalanching electrons self-replicate themselves due to either photoionization feedback [16] or due to X-ray and positron feedback [17] in conventional positive corona or relativistic electron runaway discharges, respectively.

An electron traversing the vacuum gap with potential difference  $U$  acquires maximum energy  $eU$  and generates

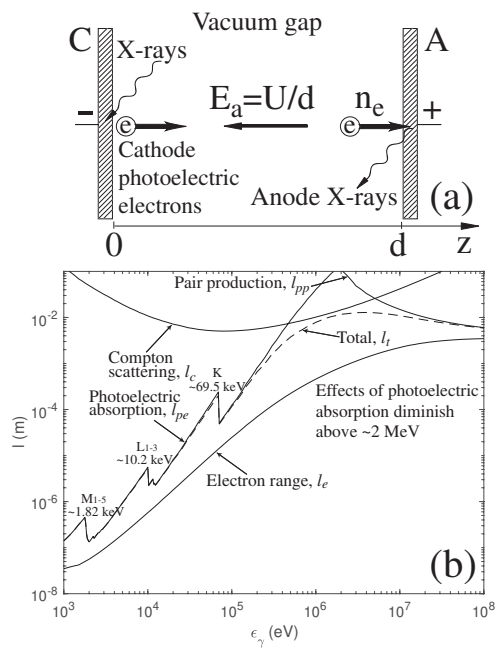


FIG. 1. (a) Schematics of simulation domain and principal physical processes. (b) Attenuation lengths of photons and electrons in tungsten.

bremsstrahlung photons from the anode with a broad energy spectrum below  $eU$ . A photon group with energy close to  $eU$  releases electrons with the same energy from the cathode (if  $eU$  greatly exceeds the work function of the cathode) upon photoelectric absorption in the cathode material. These new electrons possess energies up to  $2eU$  upon arrival at the anode surface, and the subsequent cycles can lead to further energy growth. There is a significant controversy in the existing literature as to possibility of acceleration of runaway electrons above  $eU$

in high voltage discharges (see discussion in [7, 10, and references therein]). The discharge may create regions of enhanced electric field that move synchronously with run-away electrons allowing them to gain more energy than  $eU$  as proposed in [18, 19, and references therein]. Our new findings detailed below provide an alternative mechanism.

The geometry of one dimensional coordinate  $z$  dependent model is depicted in Fig. 1(a). The electrons are assumed to start with zero energy at the cathode surface and move through vacuum gap with electrode separation  $d$  under application of constant electric field with magnitude  $E_a=U/d$ . The bombarding energy of all electrons arriving at the anode during this first passage is  $eU$ . The model accounts for different anode penetration distances of electrons  $l_e$  depending on their energy  $\varepsilon$ . In this letter the principal effects are quantitatively illustrated assuming that both cathode and anode are made of tungsten (W, atomic number  $Z_W=74$ ). The other materials used in electrode designs, i.e., aluminum, brass, copper, niobium, permalloy, stainless steel, titanium [7, 10], can be studied using the same modeling steps. The principal conclusions of this work are not affected by the electrode material. The electron range  $l_e(\varepsilon)$  data for tungsten are taken from <https://physics.nist.gov/PhysRefData/Star/Text/ESTAR.html> and illustrated in Fig. 1(b). The interaction time of electron with cathode material is estimated as  $\tau=l_e/v$ , where  $v(\varepsilon)=c\sqrt{1-(1+\varepsilon/(mc^2))^{-2}}$  is electron velocity,  $m$  is electron rest mass, and  $c$  is the speed of light in free space. The present modeling does not include consideration of characteristic X-rays. The continuous X-ray generation by electrons in tungsten is characterized by doubly differential cross-section of the bremsstrahlung photon production  $\frac{d^2\sigma_{br}}{d\varepsilon_\gamma d\Omega}$ , where the angular dependence is the one for the emitted photon [20, p. 245]; [21, p. 45, and references therein]. The X-ray emission frequency per unit energy produced by electron with energy  $\varepsilon$  [1/eV/s] is  $\nu_\gamma(\varepsilon_\gamma)=n_W \frac{d\sigma_{br}}{d\varepsilon_\gamma}(\varepsilon, \varepsilon_\gamma) v_e(\varepsilon)$  ( $\varepsilon_\gamma \leq \varepsilon$ ), where  $n_W=6.31 \times 10^{28} \text{m}^{-3}$  is tungsten number density, and  $\frac{d\sigma_{br}}{d\varepsilon_\gamma} = \int_\Omega \frac{d^2\sigma_{br}}{d\varepsilon_\gamma d\Omega} d\Omega$ . The total number of photons emitted per unit energy is  $N_{ph}(\varepsilon_\gamma)=\nu_\gamma(\varepsilon_\gamma)\tau$ . The direction of photon emission is determined by the differential cross section [20, 21] illustrated in Fig. 2(a). Only photons that are emitted toward the cathode (spherical angle  $\theta_\gamma > \pi/2$  for the reference coordinate system shown in Fig. 1(a)) are further considered. These photons are absorbed in the cathode material with the total absorption coefficient  $k_t=n_W(\sigma_{pe}+\sigma_c+\sigma_{pp})$  [ $\text{m}^{-1}$ ] that includes the photoelectric absorption, Compton scattering and pair production, with respective cross sections  $\sigma_{pe}$ ,  $\sigma_c$ , and  $\sigma_{pp}$ . Fig. 1(b) illustrates the characteristic absorption lengths of photoelectric absorption  $l_{pe}=1/(n_W\sigma_{pe})$ , Compton scattering  $l_c=1/(n_W\sigma_c)$ , pair production  $l_{pp}=1/(n_W\sigma_{pp})$ , and total absorption

$l_t=1/k_t$ . The photon cross sectional data are taken from <http://www.nist.gov/pml/data/xcom>. Probability of a photon encountering a collision after moving distance  $s$  inside of tungsten material is  $1 - e^{-s/l_t}$ . Upon collision probability of photoelectric absorption is  $l_t/l_{pe}$ . Photons advance different distances  $s$  during each step and have individual time histories. In the results reported in this letter only photons that participate in photoelectric absorption and resultant photoelectrons are followed, as Compton scattering and pair production interactions have significantly longer spatial scales (Fig. 1(b)). The kinematics of Compton scattering only produce electrons in the forward direction with respect to the incoming photon and these electrons would need to experience additional scattering interactions to be accelerated toward anode. The photons can Compton backscatter in cathode and depending on their incoming energy can contribute to population of electrons accelerating toward anode by both photoelectric absorption and Compton scattering. However, due to the original Compton scattering event having low probability and long range, we consider these effects as not dominant producers of high energy electrons. The presented modeling resolves differences between photoelectrons emitted from different shells of tungsten atom. Depending on specific shell from which electron is ejected the corresponding binding energy is subtracted from the photon energy and the remaining energy is assigned to the newly produced photoelectron. The five subshells of M shell are grouped and assigned binding energy 1.82 keV marked in Fig. 1(b). The three subshells of L shell are similarly approximated using binding energy 10.2 keV, and 69.5 keV is used for binding energy of K shell (see Fig. 1(b)). The partial cross section data for these shells are adopted from [22, 23]. The angular distribution of electrons produced in photoelectric absorption process is determined by the corresponding differential scattering cross section [24, p. 44] illustrated in Fig. 2(b). Only electrons emitted toward the anode ( $\theta < \pi/2$ ) from the cathode depth not exceeding  $l_e$  are retained for further consideration and steps discussed above are repeated. The model follows three dimensional trajectories of electrons and photons in both configuration and velocity spaces. It is expected that the adopted one-dimensional approximation (ignoring fringing effects on trajectories at the transverse edges of the discharge gap and assuming planar field geometry) is accurate with inter-electrode distance  $d$  only when the transverse area of electrodes exceeds  $d \times d$ . The differential scattering cross sections for determination of directions of bremsstrahlung photons and photoelectrons are applied in the frame of reference corresponding to incoming electron and photon, respectively, and the obtained directions are then converted to the laboratory system of coordinates depicted in Fig. 1(a) for determination of respective  $\theta$  angles discussed above. The transport and scattering of electrons and photons are modeled using

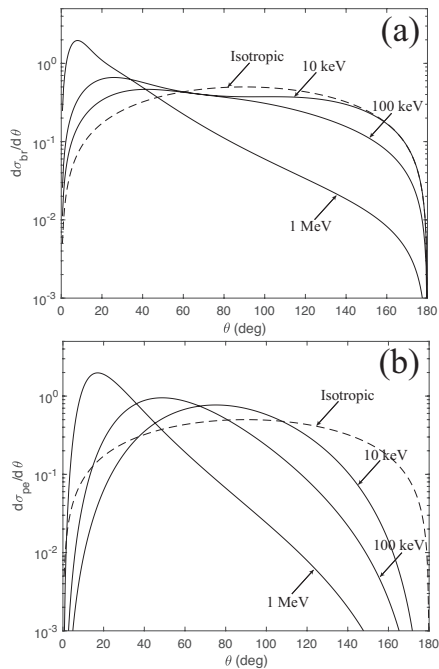


FIG. 2. (a) The normalized to unity differential cross section ( $\int_0^\pi \frac{d\sigma_{br}}{d\theta} d\theta=1$ ) defining angular distribution of bremsstrahlung photons at selected electron energies [20, p. 245]; [21, p. 45, and references therein]. For reference the dashed line shows the isotropic distribution. (b) The normalized to unity differential cross section ( $\int_0^\pi \frac{d\sigma_{pe}}{d\theta} d\theta=1$ ) defining angular distribution of electrons produced by the photoelectric absorption at selected photon energies [24, p. 44]. For reference the dashed line shows the isotropic distribution.

standard Monte Carlo techniques (details of numerical implementation can be found in [21, 25–27]).

We show representative results for two applied voltages  $U=100$  kV and  $U=1$  MV. Fig. 3(a) and Fig. 3(b) illustrate normalized to unity electron energy distribution function  $f(\varepsilon)$  of electrons arriving at the anode surface corresponding to second and third passage of electrons through the gap, respectively. We note that during the first passage (not shown for the sake of brevity) all model electrons gain energy  $eU$ . Typically  $10^8$  model electrons are used and simulations are repeated 100 times for each model voltage and differential cross section case to obtain convergent average results shown in Fig. 3. During the second passage electrons with energies exceeding  $eU$  by a factor of two are produced (Fig. 3(a)), and during the third passage electrons with energies exceeding  $2.5eU$  are observed (Fig. 3(b)). The total numbers of electrons with respect to their initial value during the second passage are 0.85% and 8.48% for  $U=100$  kV and  $U=1$  MV cases, respectively. The mean energies of these distributions are  $1.0729eU$  and  $1.01680eU$ , respectively. The total numbers of electrons with respect to their initial value during the third passage are 0.008% and 0.72%

for  $U=100$  kV and  $U=1$  MV cases, respectively. The mean energies of these distributions are  $1.0747eU$  and  $1.01678eU$ , respectively. Although in both cases very high (exceeding the applied voltage by a factor  $\sim 2.5$ ) energy electrons are produced, the mean energy of the entire electron population exceeds the applied voltage by only 1 to 7% for the model cases considered. The number of electrons in high energy electron group is estimated in different experiments to be in the range  $10^9$ - $10^{12}$  [7, 10, 15]. The presented modeling indicates that this high energy group represents only a small fraction of total electron population. For  $U=1$  MV case, electrons bombarding the anode produce significantly more bremsstrahlung photons and this directly translates to significantly higher numbers of observed photoelectrons during the second and third passages, in comparison with the  $U=100$  kV case. The majority of these photons and resultant photoelectrons reside at low energies. This enhancement at low energies also defines notably faster fall off of the tail of the normalized distribution for  $U=1$  MV in comparison with the  $U=100$  kV case seen in Fig. 3(a) and Fig. 3(b). The results for  $U=1$  MV in Fig. 3(b) indicate even faster drop off of the distribution above  $\sim 2$  MeV energy that can be directly attributed to diminishing of the photoelectric absorption in comparison with the Compton scattering and pair production as seen in Fig. 1(b) at these energies. The fact that majority of bremsstrahlung photons reside at low energies is qualitatively consistent with effective measured X-ray energies being only 9-15 keV under applied voltages 160-180 keV that produced a group of fast 340-360 keV electrons in experiments reported in [15].

Crosses in Fig. 3 show calculations for all cases that are repeated with isotropic differential cross sections for the bremsstrahlung photons (illustrated in Fig. 2(a)) and photoelectrons (illustrated in Fig. 2(b)). These results demonstrate overall tendency of reduction of the fraction of high energy electrons due to the preferentially forward emission of photons and electrons at high energies for realistic anisotropic cross sections (shown by open circles in Fig. 3) in comparison with isotropic ones, as expected. We note, however, that the electrons and photons arrive at the electrode surfaces at variety of angles, i.e. the trajectories are not necessarily normal to the surfaces. Therefore, the respective bremsstrahlung photons and photoelectrons are launched in a broad range of angles around the normal to the originating electron or photon trajectories and still may have optimal conditions to participate in the energy amplification process discussed in this letter due to much stronger differential scattering cross sections around  $90^\circ$ , as compared to backward directions around  $180^\circ$  as can be seen in Fig. 2(a) and Fig. 2(b). The effects discussed in this letter are expected to be enhanced for large area cathodes and anodes. This is generally consistent with experimentally observed reduction in numbers of high energy electrons

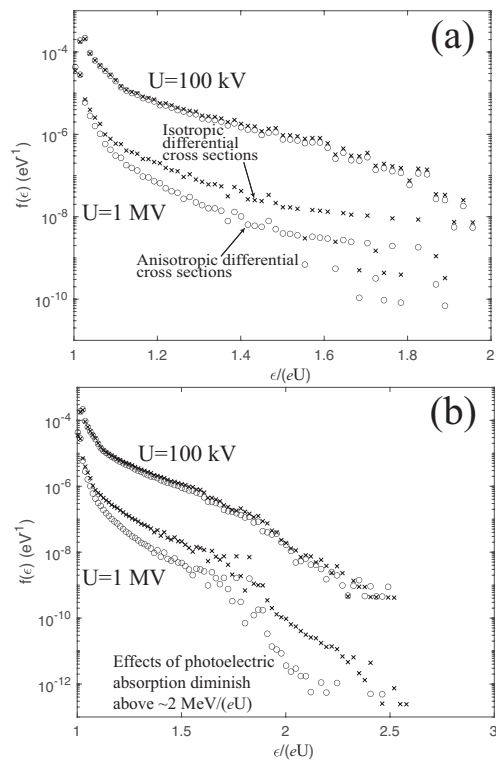


FIG. 3. Normalized to unity electron energy distribution function  $f(\varepsilon)$  corresponding to second (a), and third (b) passage of electrons through the gap.

in the following order of electrode geometries as summarized in [7]: spherical with large radius of curvature, tubular, and needle. Additionally, a high  $Z$  materials with sufficient depth exceeding the stopping distances  $l_e$  for electron energies of interest should be optimal for the anode. In tungsten  $l_e \simeq 0.5$  mm at 1 MeV and  $l_e \simeq 25$   $\mu$ m at 100 keV (Fig. 1(b)). Any shielding components made of lead (Pb,  $Z_{Pb}=82$ ) placed in the vicinity of anode may enhance the discussed feedback. We note that steel walls of experimental chamber [15] or steel ground electrode [9] may also create favorable conditions for these effects. In experiments reported in [4] it was noted that X-rays were produced from the electromagnetic compatibility (EMC) cabinet. We further comment on  $Z$  scaling below.

We briefly discuss  $Z$  scaling using iron Fe ( $Z_{Fe}=26$ ) and aluminum Al ( $Z_{Al}=13$ ). Under the identical conditions to those discussed for tungsten W ( $Z_W=74$ ) the numbers of high energy electrons are sharply reduced with reduction of atomic number. The total numbers of electrons with respect to their initial value during the second passage are 0.16% for Fe and  $1.54 \times 10^{-2}$ % for Al for the 100 kV applied voltage case, and 1.38% for Fe and 0.12% for Al for the 1 MV case. For iron the maximum observed electron energies during the third passage are  $2.25eU$  for 100 kV, and  $1.89eU$  for 1 MV. For aluminum the corresponding energies are  $1.85eU$  for 100 kV, and  $1.54eU$

for 1 MV. The longer stopping distances  $l_e$  for lower  $Z$  numbers (these scale approximately as  $Z^{-1}$ ) enhance the feedback effects discussed in this letter. However, the  $Z^2$  scaling of bremsstrahlung emissions reduces these effects for lower  $Z$  numbers. In the region of low energies 1-10 keV, where most of photons reside, the photoelectric cross sections of W, Fe and Al have complicated structure defined by L and M absorption edges of W and K absorption edges of Fe and Al. In some regions of this energy interval the cross sections are comparable, and in other regions the maximum differences do not exceed one order of magnitude. These  $Z$  trends explain observed reductions in overall percentages of high energy electrons for Fe and Al in comparison with W. In the high energy tail of these distributions (i.e., at 100 keV) the photoelectric cross sections are different by orders of magnitude (scale approximately as  $Z^4$ ) and this explains the observed sharp disappearance of high energy electrons with reduction of  $Z$  number. Interested readers can view these trends in [24, Fig. 2.5]. Therefore, in terms of material properties the effects discussed in this letter are expected to be enhanced for large  $Z$  values. The original work [15] used tungsten alloy hemispheric cathode with 12-14 mm diameter and 3-7 mm radius of curvature that appears to be favorable in terms of the geometrical and  $Z$  factors discussed above. It is noted in [7] that stainless steel cathode provided highest current of runaway electrons in comparison with other materials studied. We speculate that an admixture of small percentage (<10%) of Molybdenum Mo ( $Z_{Mo}=42$ ) in stainless steel may have contributed to the observed effects. The X-ray emissions produced by runaway electrons were observed for copper Cu ( $Z_{Cu}=29$ ) hemispherical cathodes in [6, 9]. Other favorable cathode materials for the feedback effects discussed here may include tin Sn ( $Z_{Sn}=50$ ), platinum Pt ( $Z_{Pt}=78$ ), and gold Au ( $Z_{Au}=79$ ).

It has been suggested in existing literature that photon pileup effect may be responsible for registration of X-rays with energies exceeding the applied voltage [4, 6]. The X-ray pulses can be much shorter than the detector response and pile-up effects cannot always be discounted when large deposited energies are seen. In experimental setups similar to [15] spatial filters are employed that only allow passage of high energy electrons before their detection. This provides a high degree of confidence that electrons with energies significantly exceeding  $eU$  have indeed been produced in these discharges. It is also remarkable that in [15] for the fixed gap size the number of these high energy electrons exhibited very weak dependence on air pressure over very broad range of values 0.1-760 Torr. In our modeling reported in this letter we adopted a vacuum gap to demonstrate that the electron energy amplification is likely produced due to the electrode photoelectric feedback. We emphasize that in a vacuum gap electrons with any initial energy can be viewed as runaway electrons and our work reported in

this letter does not address the sourcing of these runaway electrons. These electrons are likely produced due to the electron field emission from the cathode (see discussion in [7, 10]) as original photographs of the beam of fast electrons taken beyond the anode also demonstrate [15]. The ability to accelerate these electrons is impeded by gas in the discharge volume. The related stopping powers increase proportionally to  $Z$ , consistent with diminishing of number of fast electrons in the following order for gases studied in [15]: helium, deuterium, air, argon and xenon. The likely reasons why in experiments the runaway electrons appear when high negative polarity voltage is applied to a sharp electrode are: (1) the runaway electrons are produced from the cathode as mentioned above and have a direction of motion that allows them to effectively gain energy in near electrode region where the most of potential drop occurs; (2) in comparison with the positive polarity discharges the negative discharges develop at higher applied voltages allowing them to buildup sufficient field for development of runaway electrons [28]. X-ray emissions have been observed in positive polarity discharges. The positive discharges developing under 1 MV voltages applied over 1 m ambient air gap exhibited ten fold increase in X-ray occurrence when a fakirs bed (aluminum sheet with sharp dots) was installed on the grounded electrode that stimulated emergence of negative streamers [29]. In this regard we also note that at higher voltages the pair-production leading to generation of electron-positron pairs ( $\epsilon_\gamma \geq 1.022$  MeV [30]) and generation of neutrons ( $\epsilon_\gamma \geq 10.55$  MeV [31]) become energetically feasible. The amplification of energy of electrons and photons discussed in this letter may lead to measurable effects related to generation of electron positron pairs and neutrons and need to be investigated.

This research has been supported by the United States National Science Foundation under grant AGS-2341623 to Penn State University. S Celestin acknowledges support from the French space agency (CNES) within the projects OREO and STRATELEC, by the French Region Centre-Val-de-Loire, and by the Institut Universitaire de France (IUF).

---

\* vpasko@psu.edu

- [1] Y. L. Stankevich and V. G. Kalinin, Fast electrons and X-ray radiation during the initial stage of growth of a pulsed spark discharge in air, *Soviet Physics, Doklady* **12**, 1042 (1967).
- [2] M. Rahman, V. Cooray, N. A. Ahmad, J. Nyberg, V. A. Rakov, and S. Sharma, X rays from 80-cm long sparks in air, *Geophys. Res. Lett.* **35**, L06805 (2008).
- [3] J. R. Dwyer, Z. Saleh, H. K. Rassoul, D. Concha, M. Rahman, V. Cooray, J. Jerauld, M. A. Uman, and V. A. Rakov, A study of X-ray emission from laboratory sparks in air at atmospheric pressure, *J. Geophys. Res.* **113**, D23207 (2008).
- [4] C. V. Nguyen, A. P. J. van Deursen, and U. Ebert, Multiple X-ray bursts from long discharges in air, *J. Phys. D: Appl. Phys.* **41**, 234012 (2008).
- [5] P. O. Kochkin, A. P. J. van Deursen, and U. Ebert, Experimental study on hard X-rays emitted from metre-scale negative discharges in air, *J. Phys. D: Appl. Phys.* **48**, 025205 (2015).
- [6] C. L. da Silva, R. M. Millan, D. G. McGaw, C. T. Yu, A. S. Putter, J. LaBelle, and J. Dwyer, Laboratory measurements of X-Ray emissions from centimeter-long streamer corona discharges, *Geophys. Res. Lett.* **44**, 11174 (2017).
- [7] V. Tarasenko, Runaway electrons in diffuse gas discharges, *Plasma Sources Sci. and Technol.* **29**, 034001 (2020).
- [8] E. V. Parkevich, K. V. Shpakov, I. S. Baidin, A. A. Rodionov, A. I. Khirianova, T. F. Khirianov, Y. K. Bolotov, M. A. Medvedev, V. A. Ryabov, Y. K. Kurilenkov, and A. V. Oginov, Streamer formation processes trigger intense X-ray and high-frequency radio emissions in a high-voltage discharge, *Phys. Rev. E* **105**, L053201 (2022).
- [9] L. Contreras-Vidal, C. L. da Silva, and R. G. Sonnenfeld, Production of runaway electrons and X-rays during streamer inception phase, *J. Phys. D: Appl. Phys.* **56**, 055201 (2023).
- [10] G. V. Naidis, V. F. Tarasenko, N. Y. Babaeva, and M. I. Lomaev, Subnanosecond breakdown in high-pressure gases, *Plasma Sources Sci. and Technol.* **27**, 013001 (2018).
- [11] J. A. Seibert, X-Ray imaging physics for nuclear medicine technologists. Part 1: Basic principles of X-ray production, *J. Nucl. Med. Technol.* **32**, 139 (2004).
- [12] J. A. Seibert and J. M. Boone, X-Ray imaging physics for nuclear medicine technologists. Part 2: X-ray interactions and image formation, *J. Nucl. Med. Technol.* **33**, 3 (2005).
- [13] J. T. Bushberg, J. A. Seibert, E. M. L. Jr., and J. M. Boone, *The Essential Physics of Medical Imaging*, 4th ed. (Lippincott Williams & Wilkins, 2020).
- [14] V. P. Pasko, S. Celestin, A. Bourdon, R. Janalizadeh, and J. Jansky, Conditions for inception of relativistic runaway discharges in air, *Geophys. Res. Lett.* **50**, e2022GL102710 (2023).
- [15] L. V. Tarasova, L. N. Khudyakova, T. V. Loiko, and V. A. Tsukerman, Fast electrons and X rays from nanosecond gas discharges at 0.1-760 Torr, *Sov. Phys. Tech. Phys.* **19**, 351 (1974).
- [16] G. V. Naidis, Conditions for inception of positive corona discharges in air, *J. Phys. D: Appl. Phys.* **38**, 2211 (2005).
- [17] J. R. Dwyer, A fundamental limit on electric fields in air, *Geophys. Res. Lett.* **30**, 2055 (2003).
- [18] G. A. Askaryan, Acceleration of particles by the edge field of a moving plasma point that intensifies the electric field, *Sov. Phys. JETP Lett.* **1**, 97 (1965).
- [19] L. P. Babich, A new type of ionization wave and the mechanism of polarization self-acceleration of electrons in gas discharges at high overvoltages, *Sov. Phys. Dokl.* **27**, 215 (1982).
- [20] W. Heitler, *The Quantum Theory of Radiation*, 3rd ed. (Clarendon, Oxford, 1954).
- [21] N. G. Lehtinen, *Relativistic runaway electrons above thunderstorms*, Ph.D. thesis, Stanford University, Stanford, CA (2000).
- [22] J. H. Scofield, *Theoretical Photoionization Cross Sections*

- from 1 to 1500 keV*, Tech. Rep. UCRL-51326 (Lawrence Livermore National Laboratory, 1973).
- [23] C. Kalha, N. Fernando, and A. Regoutz, *Digitisation of Scofield Photoionisation Cross Section Tabulated Data* (Figshare Dataset, <https://doi.org/10.6084/m9.figshare.12967079.v1>, 2020).
- [24] N. J. Carron, *An Introduction to the Passage of Energetic Particles through Matter* (Taylor and Francis, Boca Raton, FL, 2007).
- [25] G. D. Moss, V. P. Pasko, N. Y. Liu, and G. Veronis, Monte Carlo model for analysis of thermal runaway electrons in streamer tips in transient luminous events and streamer zones of lightning leaders, *J. Geophys. Res.* **111**, A02307 (2006).
- [26] O. Chanrion and T. Neubert, A PIC-MCC code for simulation of streamer propagation in air, *J. Comput. Phys.* **227**, 7222 (2008).
- [27] N. Østgaard, T. Gjesteland, J. Stadsnes, P. H. Connell, and B. Carlson, Production altitude and time delays of the terrestrial gamma flashes: Revisiting the Burst and Transient Source Experiment spectra, *J. Geophys. Res.* **113**, A02307 (2008).
- [28] S. Celestin and V. P. Pasko, Energy and fluxes of thermal runaway electrons produced by exponential growth of streamers during the stepping of lightning leaders and in transient luminous events, *J. Geophys. Res.* **116**, A03315 (2011).
- [29] P. O. Kochkin, C. V. Nguyen, A. P. J. van Deursen, and U. Ebert, Experimental study of hard X-rays emitted from metre-scale positive discharges in air, *J. Phys. D: Appl. Phys.* **45**, 425202 (2012).
- [30] M. S. Briggs, V. Connaughton, C. Wilson-Hodge, R. D. Preece, G. J. Fishman, R. M. Kippen, P. N. Bhat, W. S. Paciesas, V. L. Chaplin, C. A. Meegan, A. von Kienlin, J. Greiner, J. R. Dwyer, and D. M. Smith, Electron-positron beams from terrestrial lightning observed with Fermi GBM, *Geophys. Res. Lett.* **38**, L02808 (2011).
- [31] B. E. Carlson, N. G. Lehtinen, and U. S. Inan, Neutron production in terrestrial gamma ray flashes, *J. Geophys. Res.* **115**, A00E19 (2010).